Quaternary Ammonium-Functionalized Poly(Arylene Ether Sulfone) Random Copolymers For Direct Air Capture

Hoda Shokrollahzadeh Behbahani¹, Husain Mithaiwala¹, Horacio Lopez Marques², Winston Wang², Benny D. Freeman², Matthew D. Green¹*

KEYWORDS: Climate change, Direct air capture, Moisture swing, Polysulfone, Quaternary ammonium

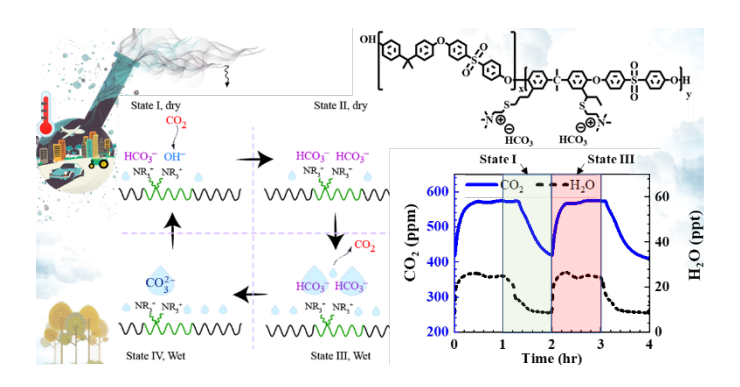


Image for Table of Contents use only.

ABSTRACT:

Direct air capture (DAC) is a promising tool for reducing CO₂ concentrations in the atmosphere and fighting climate change. We synthesized a series of quaternary ammonium (QA) functionalized poly(arylene ether sulfone) copolymers with varying mole fractions of charge content and demonstrated their potential as sorbents for DAC. Molecular weight analysis determined high monomer conversion was achieved in <6 h and relatively high molecular weights for all copolymer compositions. Thermal analysis revealed all polymers had degradation temperatures >240 °C and a single glass transition temperature (Tg); the Tg decreased with an increase in ion exchange capacity (IEC). Fractional free volume and water uptake percentage increased with the number of QA sites when compared to a neutral, commercially available polysulfone (Udel® P-1700 PSU). Next, the novel series of ammonium-functionalized copolymers exhibited a moisture-mediated capture and release of atmospheric CO₂. When exposed to air containing

¹Department of Chemical Engineering; School for Engineering of Matter, Transport and Energy, Arizona State University, Tempe, AZ 85287, USA

² John J. McKetta Jr. Department of Chemical Engineering, The University of Texas at Austin, 200 E. Dean Keeton Street, Austin, TX, 78712, USA

^{*}Corresponding author

30% relative humidity the polymers captured CO₂ and the capacity increased with the IEC. When the relative humidity was increased to 95% the samples released the CO₂. This study demonstrates a promising CO₂ DAC sorbent and highlights the possibility for continuous DAC with purpose-built free-standing membranes.

1. INTRODUCTION:

Rising global temperatures have been linked to the increase and accumulation of anthropogenic CO₂ emissions.¹ Preventing emissions and sustainably removing CO₂ are therefore paramount, especially to prevent the upcoming catastrophes predicted by the Intergovernmental Panel on Climate Change (IPCC).^{2,3} Many technologies have been developed to lower CO₂ emissions,⁴⁻⁶ but these developed processes mostly focus on capturing CO₂ from large stationery sources such as fossil fuel plants, cement plants, oil refineries, etc. Widely distributed emissions from non-stationery sources such as transportation, the built environment, waste handling, agriculture and deforestation are neglected.^{7,8} In 2019, the share of global CO₂ emissions solely from transportation and the built environment was estimated to be 25% and 38% of the total CO₂ emitted, respectively.⁹⁻¹¹ Direct Air Capture (DAC) technology is a promising approach that targets CO₂ in the ambient atmosphere and would complement traditional CO₂ capture technologies for stationary, high concentration sources. Specifically, DAC can target mobile/distributed CO₂ emissions and can potentially avoid the costs and energy requirements of CO₂ compression for transportation since installations are mobile and/or not location specific.¹² The CO₂ that is captured using DAC can be transformed into sustainable, net-zero fuels, used in the food and beverage industry, to support agriculture, mineralized, or injected deep into the ground to be permanently stored.¹³

The low atmospheric CO₂ concentration poses sorbent and capture process design challenges for DAC.¹⁴ The sorbent and/or process technology as well as the local energy source utilized could make removing CO₂ from ambient air energy intensive and create a new source of CO₂ pollution. Sorbents and capture technology designed for point source capture have to be reimagined to be useful for DAC, as CO₂

concentrations in air (~ 0.04%) are more than 300-fold lower than CO₂ concentrations in point source exhaust streams (15% – 60%). ¹⁵ Moisture swing CO₂ sorption (MSS) was first introduced by Lackner as a viable method for DAC and was further studied with experimental and computational modeling work by Yang et al. and Shi et al. 16-20 In the MSS process, CO₂ is captured by a chemisorption process. However, with the addition of a second sorbate, water (humidity), the CO₂ affinity for the sorbent changes, and the adsorbed CO₂ is released, creating something of a compromise between physisorption and chemisorption mechanisms. The process is not a competitive binding wherein water displaces a bound CO₂, but rather the sorbed water modifies the hydration of the bound carbonaceous species and alters the sorbent-CO₂ affinity. In thermodynamic analysis, the free energy required for regeneration is provided by water evaporation, so a swing in moisture replaces the conventional thermal or pressure swings used for sorbent regeneration.²¹ The simplified MSS mechanism is illustrated in **Figure 4** for a polymer with positively charged quaternary ammoniums (QA) neutralized with hydroxide (OH⁻), bicarbonate (HCO₃⁻), or carbonate (CO₃²⁻) ions. In "dry" conditions, the carbonate-bicarbonate equilibrium favors the presence of hydroxide and bicarbonate ions since carbonate ions are less stable. This is shown as state I in Figure 4. The CO2 in the atmosphere reacts with the hydroxide forming a bicarbonate saturated sorbent (state II). Due to the high affinity of CO₂ for hydroxide, this reaction occurs even at atmospheric CO₂ partial pressures. When humidity is introduced, the bicarbonate is hydrated (state III) and dissociates to release CO₂ to the environment, leaving the surface saturated with carbonates stabilized by water (state IV). Destabilization of carbonate occurs during a reduction in water activity, returning to state I, and the MSS cycle is closed. The MSS is also demonstrated through Equation 1, where R^+ , x and y represent the QA groups, moles of water associated with bicarbonate, and moles of water associated with carbonate, respectively.²²

$$2(\mathrm{HCO_3^-}\,\mathbf{R}^+.xH_2O) + (\mathrm{y} - 2\mathrm{x} - 1)\mathrm{H}_2\mathrm{O}_{(g)} \ \leftrightarrow \mathrm{CO_3^{2-}}(\mathbf{R}^+)_2.yH_2O + CO_{2(g)} \tag{Eq. 1}$$

DAC researchers have studied the applicability of a variety of materials with quaternary ammonium groups for the moisture-swing sorption process. However, comprehensive investigations are still required to better understand the mechanism, develop faster kinetics, increasing loading capacity, and enhance

selectivity for CO₂.²³ Porous polymers, ammonium-based anion exchange resins, ammonium-functionalized ionic liquids, cellulose and chitosan/PVA aerogels, ammonium-modified silica, colloidal crystal templates, and sorbent-containing electrospun fibers have been evaluated as sorbents.^{20,24–35,36} He and coworkers tested three QA-functionalized porous materials and reported CO₂ uptakes between 0.13–0.49 mmol/g when cycling the relative humidity between 20–95%.²⁴ Song and coworkers investigated QA chitosan/PVA and reported a maximum uptake of 0.18 mmol/g at room temperature while varying the relative humidity between 3-95%.³² Hou and coworkers studied QA-modified bamboo cellulose and reported a maximum uptake of 0.19 mmol/g at 25 °C and a RH swing between 60-80%.³¹ These investigations show that the sorption and desorption capacities for CO₂ are significantly improved compared to commercial resins by increasing porosity, gas diffusivity and reduced sorbent size. Also, most moisture-swing sorbents for DAC utilize batch-wise processes where a porous sorbent is consecutively dried and hydrated to load and unload.³⁷ Assuming the same performance, continuous CO₂ capture would be preferred over batch processes in large-scale applications. To date, continuous MSS processes investigated in literature utilize commercial anion exchange membranes and pump CO₂ through the membrane with the assistance of a potential field.^{38,39}

Potential sorbents for DAC must be robust to withstand the potentially long service life and exposure to a range of ambient conditions (e.g., seasonal temperature variations, storms, UV light, etc.). Thus, research into high polymers is gaining traction because of the favorable thermomechanical properties, scalable manufacturing, the potential to introduce macro- and/or micro-porosity, and the ability to tune the chemistry of these materials. Due to its tunability, and outstanding mechanical, thermal, and chemical properties, poly(arylene ether sulfone) PAES is a popular example of a versatile high-performance thermoplastic. Researchers have employed a variety of pre- and post-polymerization techniques to tailor the structure of PAES, achieving desired properties that align with specific application requirements. Introduction of functional groups into the PAES backbone has enabled tuning of thermal, chemical, and mechanical stability, solubility, hydrophilicity/hydrophobicity, electrical conductivity, permeability,

permselectivity, and biocompatibility. **Table S.1** illustrates examples of functionalities skillfully added to PAES such as imidazolium, sulfobetaine zwitterions, sulfonates, imides, and quaternary ammoniums. Some modification routes that can be used to introduce these functionalities include bromination, sulfonation, alkylation, chloromethylation, ring opening reactions, and "click" chemistry. Functionalized PAES finds application in membranes for water treatment and gas separation and production of industrial parts. Predominately, functionalized PAES has been studied as a proton exchange membrane material in fuel cell applications.⁴⁰ Membranes with charge densities (or ion exchange capacities (IEC)) up to ~3 mmol/g have been synthesized for this purpose.^{41,42} A brief survey of this field highlights a lack of investigations into these promising materials and their utility for DAC.

Herein, a novel QA-functionalized poly(arylene ether sulfone) random copolymer (PAES-co-QAPAES) is prepared for DAC. The ammonium groups are added to a polysulfone backbone through post-polymerization modification of an allyl-modified poly(arylene ether sulfone) (PAES-co-APAES) to leverage the excellent mechanical strength, high thermal and chemical stability, and processibility of polysulfones. The ammonium cation attached to the polymer backbone is balanced by bicarbonate ions through an anion exchange process. Polymers with varying ion exchange capacities (IEC) are synthesized, characterized, and tested for MSS performance. Kinetic modeling studies evaluate the potential of this novel material to be used as a sorbent and future studies will explore these materials as processible standalone membrane that enable continuous DAC.

2. EXPERIMENTAL

2. 1. Materials and Reagents

Bisphenol A (BPA, >99%) was purchased from Sigma-Aldrich and recrystallized from acetic acid/water (1:1 v/v) before use. Bis(4-fluorophenyl) sulfone (DFDPS, 99%) was purchased from VWR and recrystallized from toluene before use. 2,2'-Diallylbisphenol A (DABA, 85%) was purchased from Sigma-Aldrich and purified by liquid-liquid extraction. ⁴⁴ Potassium carbonate (K₂CO₃, ≥99%) was purchased from Sigma-Aldrich and kept inside an oven operating at 130 °C before use. Toluene (99.8%) and THF OptimaTM were purchased from Fisher Scientific and used after passing through an MBraun SPS-800 solvent purification system. N,N-Dimethylacetamide (DMAc, 99.5%), deuterated dimethyl sulfoxide, (DMSO-d6, 99.9 atom% D, 0.03% (v/v) TMS), diatomaceous earth (Celite® 545) and 2,2-dimethoxy-2-phenylacetophenone (DMPA, 99%) were purchased from Sigma-Aldrich and used as received. 2-(Dimethylamino)ethanethiol hydrochloride (95%) and deuterated chloroform (CDCl₃, 99.8 atom% D, 0.03% (v/v) TMS) were purchased from Acros Organics and used as received. N,N-Dimethylformamide (DMF, ≥99.8%) was purchased from BDH® VWR and used as received. Hydrochloric acid (HCl, 36.5-38%) was purchased from BDH® VWR and diluted with THF before use. Iodomethane (≥99.5%) was purchased from Beantown Chemical and used as received. Narrowly distributed (Đ ~1) 200 kDa and 30 kDa polystyrene (PS) standards were purchased from Pressure Chemical Company, and 482 kDa, 91,450 Da, 9,820 Da and 4,910 Da PS standards were purchased from Agilent technologies and used as received. Udel® P-1700 NT 11 polysulfone (PSU) pellets were purchased from Solvay specialty polymers and used as received.

2. 2. Synthesis

The production of QA-functionalized poly(arylene ether sulfone) sorbent with basic counterions is a 4-step process. The first step is a step- growth reaction to form the allyl-modified poly(arylene ether sulfone) (PAES-co-APAES) copolymer, the second step is a post-polymerization modification reaction to create the tertiary amine-modified PAES (PAES-co-TAPAES) copolymer, the third step is quaternization

of the amine to form the QA-modified ((PAES)-co-[QAPAES][I]) copolymer, and the fourth step is counterion exchange ((PAES)-co-[QAPAES][HCO₃]).

PAES-co-APAES(25) was synthesized via the following established step growth reaction. 45-47 DABA (2.0 g, 6.5 mmol), BPA (4.4 g, 19.5 mmol), DFDPS (6.6 g, 25.9 mmol) and K₂CO₃ (4.3 g, 31.1 mmol) were weighed and added to a two-neck 250 mL round-bottom flask along with a magnetic stir bar. The flask was equipped with a Dean-Stark apparatus, a reflux condenser, and a nitrogen inlet/outlet and the complete apparatus was lowered into an oil bath equipped with a thermometer. Different BPA/DABA ratios were used to manipulate the charge content on the polymer backbone, and the molar ratio for other components were kept constant (e.g., DABA/BPA ratio of 3/1, 1/1 and 1/3 refer to 75%, 50% and 25% mol functionalized polymer, respectively). 52 mL DMAc was added to dissolve the monomers, and 26 mL toluene was added as an azeotropic agent to remove water during the polycondensation reaction. The solution was purged with nitrogen for 15 min, then refluxed at 135 °C for 2 h to dehydrate the reaction mixture through the water-toluene azeotrope. The mixture was then heated to 145 °C to remove the residual toluene, and the reaction was continued under static nitrogen atmosphere at 145 °C for 6 h. The reaction mixture was then cooled to room temperature and diluted with THF. The mixture was stirred with dilute HCl in THF for 2 h for neutralization to occur and pulled through diatomaceous earth to filter inorganic salts with a Büchner funnel. The polymer was then isolated through precipitation by addition, while stirring, of a 50/50 vol.% solution of DI water and methanol. The polymer was dried under vacuum at 60 °C, redissolved in THF and precipitated once again in DI water. The product, PAES-co-APAES(25), was dried under vacuum at 60 °C overnight.

The second step, which involves the incorporation of the tertiary amine functional groups via the thiol-ene "click" reaction, consisted of dissolving PAES-co-APAES(25) copolymer (11.0 g, 10.7 mmol ene), 2-(dimethylamino)-ethanethiol (7.6 g, 5 equiv. to ene) and DMPA (0.8 g, 0.3 equiv. to ene) in 70 mL DMF. ^{48,49} The mixture was poured into a 100 mL round-bottom flask, purged with nitrogen for 15 min, and irradiated with a compact UV lamp (Analytik Jena US UVL-28 EL series at 365 nm) at room temperature

for 2 h. The product (PAES-co-TAPAES(25)) was isolated by precipitation in DI water and was then dried under vacuum at 60 °C, redissolved in DMF, reprecipitated in DI water, and dried under vacuum at 60 °C overnight.

In the third step, tertiary amine groups were converted to quaternary ammoniums via the established Menshutkin reaction. To a solution of PAES-co-TAPAES(25) (10.5 g, 10.1 mmol tertiary amine) in 70 mL DMF, iodomethane (7.2 g, 5 equiv. to tertiary amine) was added. The reaction mixture was stirred at room temperature and the product (PAES-co-QAPAES(25)[I]) was isolated via precipitation in stirring DI water and then dried under vacuum at 60 °C overnight. The polymers were redissolved in DMF and reprecipitated in DI water. To substitute the iodide counterions with bicarbonate counterions, as the fourth step, PAES-co-QAPAES(25)[I] was placed inside a stirring solution of 1 M KHCO₃ in DI water at room temperature for 48 h, and then washed 3 times with DI water.

2. 3. Characterization

2.3.1. Copolymer structure

To confirm the polymer structure, ¹H NMR spectra were recorded on a Varian 500 MHz spectrometer. For this characterization, 20 mg of dried polymer was dissolved in 0.7 g of deuterated solvent.

2.3.2. Polymer molecular weight

Size exclusion chromatography (SEC) was carried out using a Waters Alliance e2695 HPLC system interfaced to a Wyatt miniDAWN TREOS light scattering detector and a Wyatt Optilab T-rEX differential refractive index (dRI) detector connected to Astra v6.1 software to determine the molecular weight of the polymers. The mobile phase was THF OptimaTM with a flow rate of 1.0 mL/min. The molecular weights of synthesized polymers were measured from a calibration curve obtained from 6 low dispersity PS. The testing solutions were prepared by dissolving polymers in THF to a concentration of 5 mg/mL and passing through a 0.45 µm filter. The cyclic oligomer content in SEC traces was measured from the ratio of area under curve of cyclic shoulder vs. the total area in the elution trace.

2.3.3. Thermogravimetric analysis (TGA)

The decomposition temperature of the synthesized polymers was investigated to evaluate the thermal stability using a TA Instruments TGA 5500. \sim 20 mg of sample was inserted into a platinum HT pan and heated up to 120 °C under nitrogen, at a rate of 10 °C/min to evaporate any water or solvents that may be present. Then, the sample was cooled to rt followed by thermal scanning up to 750 °C with the same rate under inert N_2 atmosphere. The temperature at which 5% weight loss ($T_{d5\%}$) was observed is reported as the thermal stability.

2.3.4. Differential scanning calorimetry (DSC)

To determine the glass transition temperatures (T_g) of the polymers, a TA Instruments Q2000 calorimeter was used. The polymer samples were heated under N_2 at a rate of 10 °C/min to 190 °C, held isothermally for 10 min, cooled to -80 °C, held isothermally for 10 min, and finally heated again at a rate of 10 °C/min to 200 °C. The polymer samples were loaded into a non-hermetically sealed aluminum pan, and the T_g of the polymers were determined from the midpoint T_g function in the TA instruments Universal Analysis 2000 software (Version 4.5A) from the second heating scan.

2.3.5. Water vapor gravimetric sorption

A McBain quartz spring balance was used to perform the water vapor gravimetric sorption measurements. The polymer sample was placed in a small aluminum foil pouch which is suspended from a sensitive quartz spring (Deerslayer Quartz Springs) inside a water-jacketed glass chamber at 25 °C. DI water contained in a glass reservoir was used to generate water vapor. Before the measurements, the DI water in the reservoir was degassed under full vacuum (<0.01 Torr) to remove dissolved gasses from the water. Water partial pressure was monitored using an MKS Baratron 626B transducer (full scale = 100 Torr). Prior to each test, the sample was degassed under full vacuum until no further displacement of the spring is observed. Then, sorption experiments were performed by exposing the sample to water vapor at 100% RH. The spring position was monitored using a digital camera, and the images were processed using

ImageJ software. 53,54 Blank experiments were performed and the amount of water adsorbed by the aluminum foil pouch is subtracted in all sorption experiments.

2.3.6. Polymer density, molar volume, and fractional free volume

The true density of the polymers was measured in the powder form. The polymers were dried in a vacuum oven at 50 °C for 24 h and weighed using an Accuris Instruments W3100-120 analytical balance. The volume of the samples were measured as the average of 10 volume displacements using a Micromeritics AccuPyc II 1340 Gas Pycnometer operating with helium gas.

The polymer molar volume, v (mL/mol) (**Equation 2**), was calculated by dividing the molar mass of polymer repeat unit, Mw_{ru} (g/mol) by the true density, ρ (g/mL).

$$v = \frac{Mw_{ru}}{\rho} \tag{Eq. 2}$$

The fractional free volume of polymers, f (Equation 3), where v is the molar volume, and v_0 is the volume occupied per one mole of repeat unit at 0 K (zero-point molar volume).⁵⁵ An approximation for the zero point molar volume is reported by Bondi to be 1.3 times the van der Waals volume (v_{VDW}).⁵⁶ The v_{VDW} per one mole of polymer repeat unit can be calculated by the sum of v_{VDW} of composing structural groups, and the v_{VDW} of each structural group was derived from literature.⁵⁷

$$f = \frac{v - v_0}{v} \tag{Eq. 3}$$

The v_{VDW} of Udel® P-1700, PAES-co-QAPAES[HCO $_3$](25), PAES-co-QAPAES[HCO $_3$](50) and PAES-co-QAPAES[HCO $_3$](75) is calculated to be 234.2, 1042.6, 574.2 and 1254.3 mL/mol, respectively (see **Table S.5 – S.8**, SI, for calculation).

2. 4. Sorption kinetics

For the synthesized polymers, sorption kinetics were investigated through fitting experimental sorption data (see **S.3**, Supporting Information, for information on experimental setup) with kinetic models. Pseudo

First Order (PFO)⁵⁸ (**Equation 4**) and Pseudo Second Order (PSO)⁵⁹ (**Equation 5**) models are the two main models used to described kinetics in the gas sorption processes. In these equations, q_e is the equilibrium sorption capacity (μ mol/g), q_t is the amount of sorbed CO_2 at time t (μ mol/g), k_f and k_s are the PFO and PSO rate constants (1/h), respectively.

$$q_t = q_e(1 - \exp(-k_f t)) \tag{Eq. 4}$$

$$q_t = \frac{k_s q_e^2 t}{1 + k_s q_e t} \tag{Eq. 5}$$

3. RESULTS AND DISCUSSION:

3.1. Synthesis of random QA-functionalized poly(arylene ether sulfone) copolymers

The ultimate objective in the synthesis of these QA-functionalized PAES copolymers is to maximize the ammonium content while maintaining good thermomechanical stability. The PAES copolymers are prepared using the multi-step synthetic protocol shown in Figure 1. First, the copolymer is prepared using a step-growth polymerization. The addition of allyl pendant groups on the polysulfone backbone enables post-polymerization functionalization to introduce chemical moieties and deliver new functionality to the traditional polysulfone polymer. The allyl concentration is tuned by controlling the DABA and BPA monomer ratio in the feed when performing step-growth polymerization (i.e., PAES-co-APAES(25) indicates a DABA/BPA ratio of 1/3 or 0.25 mol of DABA with respect to 1 mol of the repeat unit). Allyl functionalities (PAES-co-APAES) are then converted to tertiary amines (PAES-co-TAPAES) through the thiol-ene "click" reaction and quaternized to create QA-functionalized polysulfone polymers (PAES-co-QAPAES) using the Menshutkin reaction. Figure 1 shows the ¹H NMR spectra of Udel® P-1700 PSU (an unfunctionalized control) and our synthesized polymers. Allyl functionalities are successfully incorporated on the backbone, as seen by the appearance of peaks at 3.24, 6.21, and 4.94 ppm belonging to protons on the non-isomerized allyl group (h, g and f, respectively) and peaks at 6.47, 5.81, and 1.78 ppm corresponding to protons on the isomerized allyl group (i, j and k, respectively). These values agree with a spectrum from literature with the same polymer backbone. ⁶⁰ The ratio between the integral of peaks f-k and

peak a is used to assess the percentage of functionalization. Upon analysis, the theoretical percentage of functionalization agrees with the actual amount within $\pm 2\%$ accuracy for all allyl modified poly(arylene ether sulfones) (i.e., PAES-co-APAES(25), PAES-co-APAES(50), PAES-co-APAES(75)). The ratio between the integrals of peaks i-k to f-k is used to calculate the extent of isomerization of the allyl functionality, with 30%-60% isomerization observed for all polymers. Nonetheless, the ¹H NMR spectrum of tertiary amine-modified polysulfone (PAES-co-TAPAES in Figure 1) confirms that isomerization of the allyl group does not interfere with the extent of post-polymerization functionalization. Peaks corresponding to allyl sites completely disappear after the thiol-ene "click" reaction, and new peaks are observed at 1.15 ppm, and 2.68 - 3.91 ppm which correspond to k' and l, m, n, h', i' and j' functionalities in Figure 1. The ratio of integrals of peaks n and k' with respect to peak a validates complete conversion of the allyl group to thiol-ether with the thiol-ene "click" reaction. The molar concentration – ratio of integrals – of peaks n and k' with respect to peak a - is used to confirm that the amine concentration matches the allyl concentration noted above. Upon quaternarization of tertiary amines with methyl iodide (PAES-co-QAPAES in Figure 1), the peak at 2.68 ppm shifts to 2.75 ppm, indicating the successful conversion to quaternary ammonium. The ratio of integrals of peaks n' and k' with respect to signal a confirms full conversion and is used to calculate the experimental IEC.

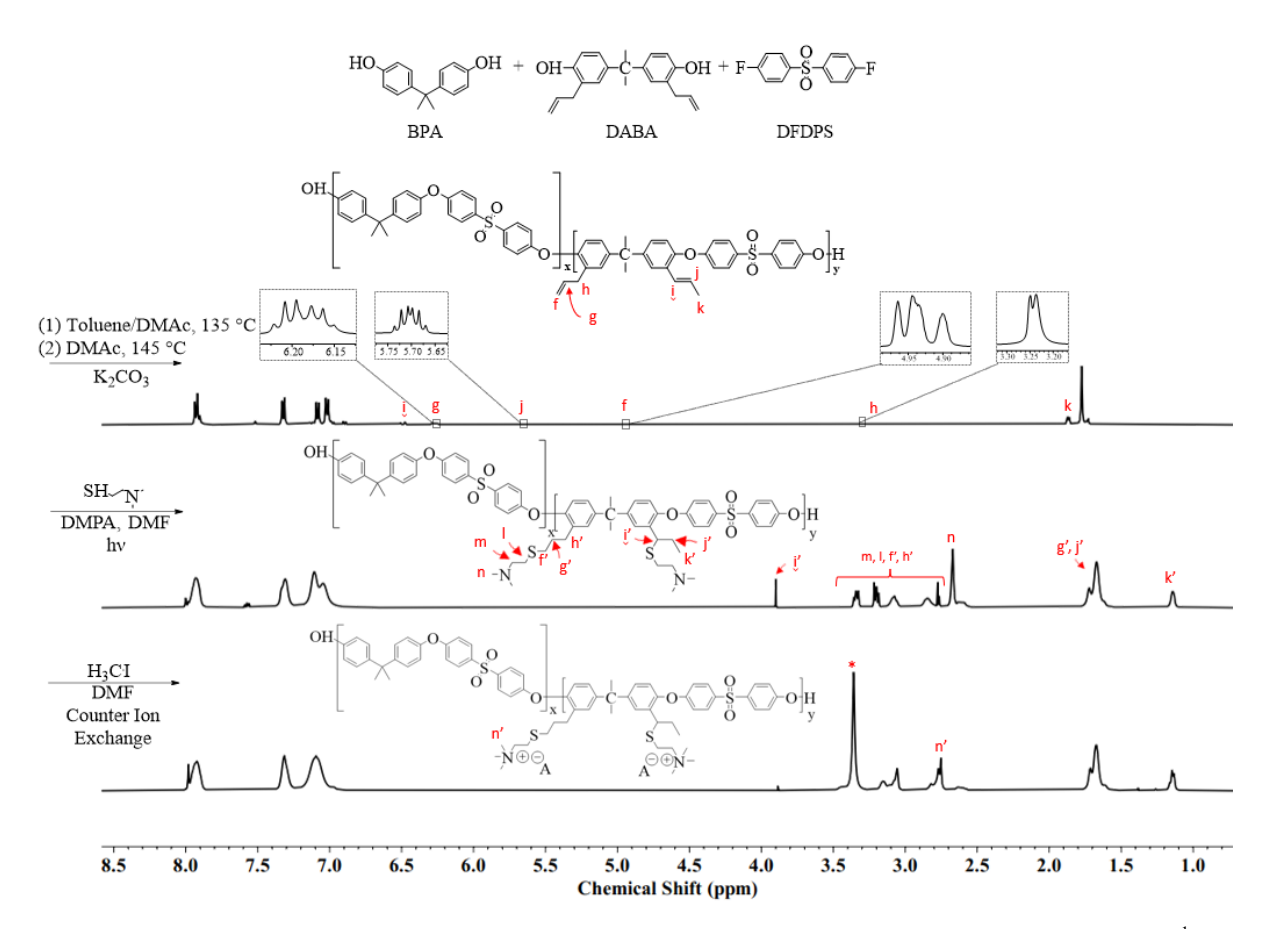


Figure 1 Reaction pathway for production of PAES-co-QAPAES[HCO₃-] and from top to bottom: ¹H NMR spectra of Udel® P-1700 PSU in CDCl₃, PAES-co-APAES(25) in CDCl₃, PAES-co-TAPAES(25) in DMSO-*d*₆, PAES-co-QAPAES(25) in DMSO-*d*₆.

An established method of counterion exchange is employed to exchange the counterion from iodide to bicarbonate. To substitute the iodide counterions with bicarbonate counterions, PAES-co-QAPAES(25)[I] was placed inside a stirring solution of 1 M KHCO₃ in DI water at room temperature for 48 h, and then washed 3 times with fresh DI water, as this protocol has proven successful in literature. A hydroxide, carbonate, or bicarbonate ion may replace iodide and the starting counterion has no effect on the outcome of MSS process. Bicarbonate ions are superior to carbonate ions for ion exchange, because carbonate's divalent charge results in a larger hydrated-ion size that is unfavorable for ion exchange. A larger hydrated-ion size obstructs its diffusion into the polymer structure. Hydroxides are less favorable than bicarbonates because they have a higher binding energy that limits transport in the polymer as well as the potential to initiate Hofmann elimination during storage, sonication, and the drying process thereby requiring a more complicated polymer preparation protocol.

The molecular weights of the allyl-modified polysulfones are determined using SEC (Figure 2). The number-average molecular weights for Udel® P-1700 PSU, PAES-co-APAES(25), PAES-co-APAES(50) and PAES-co-APAES(75) are 49.5, 23.1, 83.9, and 112.8 kDa with dispersity (θ (M_W/M_n)) values of 1.5, 1.8, 2.1, and 2.4, respectively. High molecular weights are achieved thanks to extensive monomer purification and low reaction times are attributed to the use of DFDPS in the step-growth reaction. ⁴⁷ The SEC traces of all polymers (**Figure 2-a**) show a bimodal molecular weight distribution with a low molecular weight shoulder attributed to the generation of lower molecular weight cyclic compounds (See Table S.2 in the SI for a summary of molecular weight analyses performed with and without the low molecular weight shoulder in the elution profile). Cyclic oligomers can form from the reaction between the phenoxide and aryl halide end groups on the low molecular weight oligomers during in the step growth reaction. 66,67 The use of DABA as a comonomer introduces concerns over cross-linking, as the unsaturated allyl groups can react through a number of different reaction pathway. The absence of a shoulder at the lower elution times in all SEC traces (Figure 2-a) indicates cross-linking did not occur. According to the classical theory by Carothers and Flory, the D of polymers in step-growth reaction will equal 2.0 when complete conversion of monomers is attained.^{68,69} However, further investigations into the step-growth reaction showed cyclic compounds are generated at any chain length during step-growth polymerization and compete with linear chain growth.³⁹ This influences the value of D, yielding higher values (D = 2-20) at higher conversions without fractionation of polymers to remove cyclic compounds before SEC analysis. 66,70,71 As an example, a mathematical study on step-growth reaction for aliphatic chains with alkane moieties generated \mathcal{D} of 2.77 at 98% conversion. ⁷² Another mathematical study observed \mathcal{D} >20 at 100% polycondensation reaction between silylated conversion the tetrahydroxytetramethylspirobisindane with 1,4-dicyanotetrafluorobenzene.⁷³ A series of experimental studies carried out by Kricheldorf et al. for step-growth reactions of aromatic monomers yielded D values between 3-15 at above 97% conversion. 74–76 Thus, high \mathcal{D} values obtained are validated and show high reactant conversion. The cyclic content (weight fraction) in Udel® P-1700 PSU, PAES-co-APAES(25), PAES-co-APAES(50) and PAES-co-APAES(75) is calculated to be 1.7%, 5.2%, 5.7% and 20.9%, respectively (see Table S.2, SI, for calculation). An increasing trend in cyclic content is observed with increasing DABA content, which we think may be due to a higher propensity for reaction between telechelic end groups on the low molecular weight oligomer chains in the step-growth reaction. This reaction may be the result of greater segmental motion caused by added free volume from the pendant allylic groups on DABA. Alternatively, increased steric hinderance in the step growth reaction for DABA addition could cause slower reaction rate constants for DABA compared to BPA. Thus, at higher DABA content, the propensity for side reactions would be higher. Interestingly, for polymerizations with the same reaction time (6 h) and identical synthesis protocols, a higher DABA/BPA ratio results in a higher molecular weight. Future kinetic and viscosity studies will better understand this trend. The combination of molecular weight data from SEC and ¹H NMR spectra confirms the successful synthesis of high molecular weight QA-functionalized poly(arylene ether sulfones).

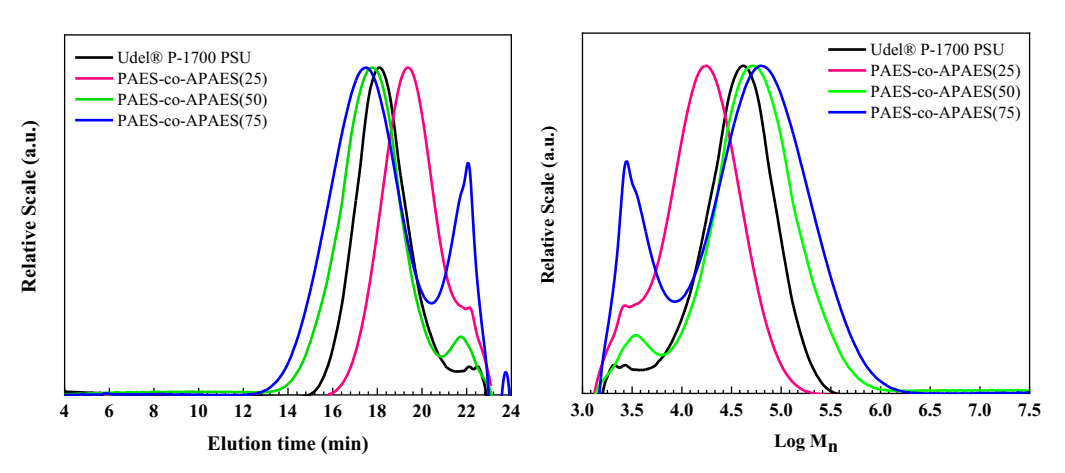


Figure 2 SEC traces of a) elution time b) Log M_n for Udel® P-1700 PSU, PAES-co-APAES(25), PAES-co-APAES(50) and PAES-co-APAES(75)

3.2. Thermogravimetric analysis (TGA) and Differential Scanning Calorimetry (DSC) of the synthesized random copolymers

The thermal stability of the polymers is studied using TGA as shown in **Figure 3**. Udel® P-1700 PSU exhibits a one-step weight loss at ~470 °C, corresponding to backbone degradation⁷⁷. The QA-functionalized polysulfones remain stable up to a temperature of ~120 °C and show a multi-step weight loss with onset temperatures of 122-127 °C, 203-211 °C, 330-384 °C and ~470 °C, as shown as a, b, c, and

d in the 1st derivative plot in **Figure 3**. The first weight loss is the evaporation of solvent (DMF) and water held by the counterion. The next steps are the chemical degradation of counterions and initiation of Hofmann elimination by the alkaline counterion, degradation of sulfur bonds (-S-) and decomposition of the main chain. As also observed in literature, all polymers show a large residual mass (25-30%) at 800 °C, which is due to the large number of aromatic compounds. The multi-step weight loss observed agrees with TGA profiles reported in literature for similarly functionalized backbones. All The $T_{d5\%}$ of QA-functionalized polysulfone copolymers is 241-262 °C, which is ~53% lower than Udel® P-1700 PSU as a result of the ammonium groups. However, these values are still well beyond atmospheric temperatures where DAC is envisioned to be conducted.

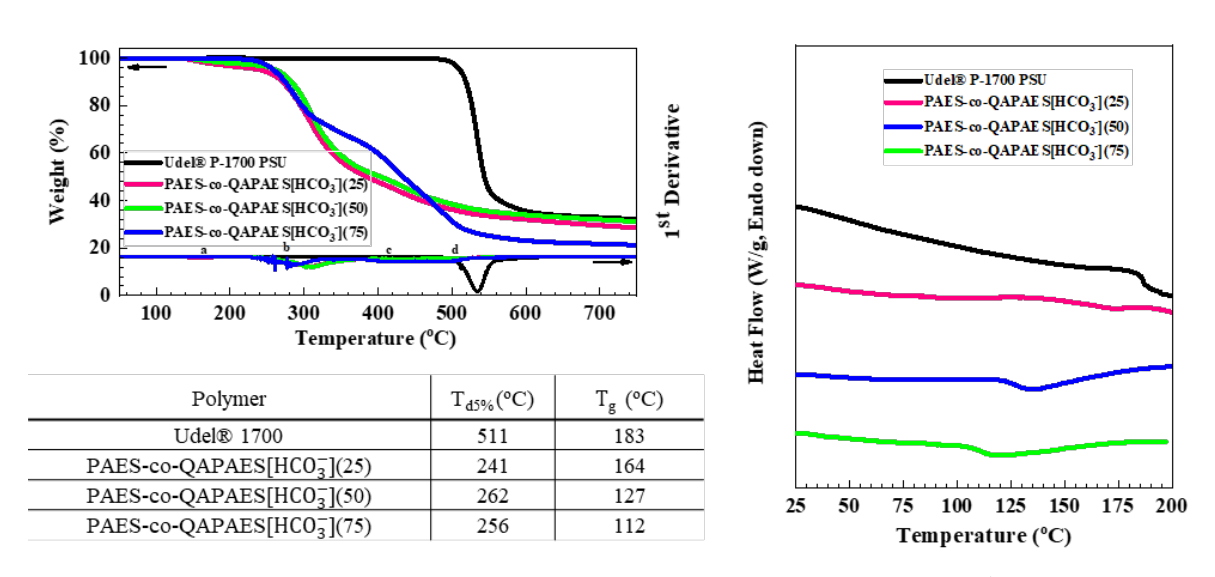


Figure 3 Thermal analysis of the QA-functionalized copolymers. TGA and 1st derivative (DTA) plot of Udel® PSU, PAES-co-QAPAES[HCO₃-](25), PAES-co-QAPAES[HCO₃-](50) and PAES-co-QAPAES[HCO₃-](75) obtained from thermal scanning up to 750 °C under N₂ and T_{d5%} of polymers (top left). DSC traces from second heating scan (shifted vertically for clarity) of from top to bottom: Udel® P-1700 PSU, PAES-co-QAPAES[HCO₃-](25), PAES-co-QAPAES[HCO₃-](50) and PAES-co-QAPAES[HCO₃-](75) (right).

The DSC thermograms and glass transition temperature (T_g) of Udel® P-1700 PSU and the synthesized QA-functionalized polysulfones are also shown in **Figure 3**. The T_g of Udel® P-1700 PSU agrees with literature.⁸² The T_g s of PAES-co-APAES(25), PAES-co-APAES(50) and PAES-co-APAES(75) are measured as 166 °C, 152 °C, and 145 °C, decreasing by 9%, 17% and 21%, respectively, in comparison to Udel® P-1700 PSU. The entanglement molecular weight (M_e) of BPA-based polysulfone

is 2,300 Da, and the molecular weight of all investigated polymers are more than 10X this value, so we are safe in neglecting the effect of molecular weight on T_g . The decrease can be due to the larger free volume between polymer chains caused by the pendant allyl functionalities causing weaker interactions. When the allyl group is converted to the quaternary ammonium a further reduction in T_g is observed. The decrease in T_g is 10%, 31% and 39% for PAES-co-QPAES(25), PAES-co-QAPAES(50) and PAES-co-QPAES(75), respectively, in comparison to the allyl copolymer precursor. The larger drop in T_g observed for QA-functionalized polysulfone compared to allyl-modified polysulfone is believed to be the result of bulkier pendant sites causing larger free volume and weaker interactions between polymer chains, which enables easier cooperative segmental motion at lower temperatures. The increase in free volume hypothesis is further supported by the fractional free volume measurement (f) for polymers reported in **Table S.4**, SI. Increases of 3.4%, 52.0% and 71.2% are observed compared to f of 0.177 for Udel® P-1700 PSU for PAES-co-QAPAES[HCO $_3$](25), PAES-co-QAPAES[HCO $_3$](50) and PAES-co-QAPAES[HCO $_3$](75), respectively (see **Table S.4** and **Tables S.5-S.8**, SI, for v and v_{VDW} , and v_{VDW} calculation, respectively).

The PAES-co-APAES data fit to the Fox equation, which estimates the T_g of random copolymers. Each pairwise set of data predicted a T_g of 143 °C for 100% APAES with ±2 °C standard deviation. Because of the agreement between the Fox equation and the experimental data, we can infer a random copolymer structure. No crystallization or melt transitions were observed in the DSC analysis, and a single T_g is observed meaning the polymers have an amorphous morphology with non-phase separated and randomly dispersed polymer segments. This is in agreement with literature, as polysulfones inhibit crystalline morphologies due to the bond angles along the backbone. Interestingly, all of the copolymers exhibited brittle mechanical properties when prepared into dense, asymmetric, or thin film composite membranes. This is an area of research we endeavor to address in future work.

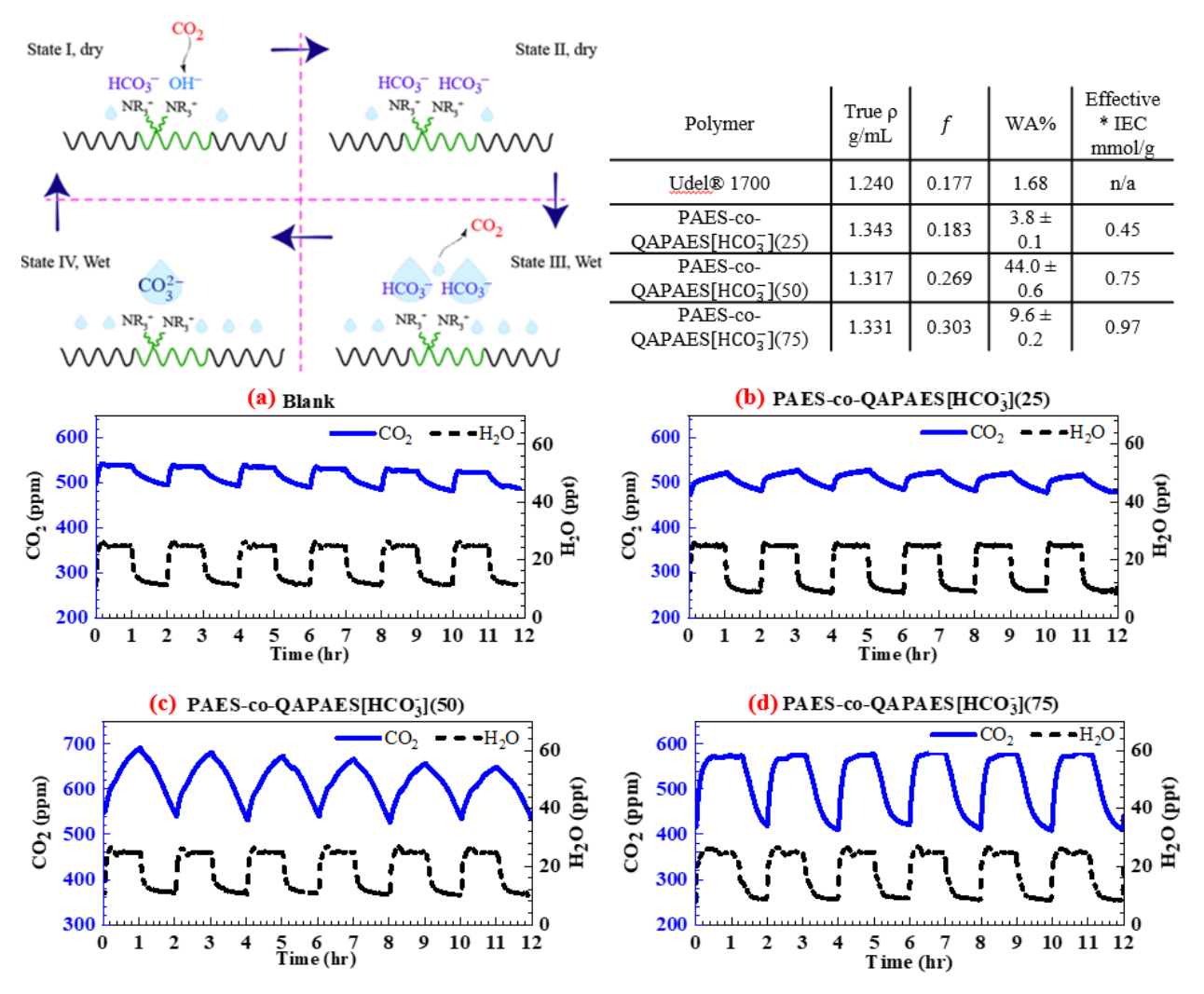
3.3. Water vapor gravimetric sorption

The results for polymer water uptake (WA) are shown in **Figure 4**. WA for Udel® P-1700 PSU, PAES-co-QAPAES[HCO₃⁻](25), PAES-co-QAPAES[HCO₃⁻](50), and PAES-co-QAPAES[HCO₃⁻](75) are 1.68%, 3.8%, 44.0%, and 9.6%, respectively. All QA functionalized polymers have higher WA than Udel® P-1700 PSU due to the addition of hydrophilic QA groups. With an increase in QA content, the WA initially increases greatly from 3.8% to 44%, then decreases to 9.6%. The initial increase is due to the presence of a higher number of hydrophilic QA regions. The decrease of 44% to 9.6% (for PAES-co-QAPAES[HCO₃⁻](50) and PAES-co-QAPAES[HCO₃⁻](75), respectively) is as ascribed to the result of random ionic clustering in the copolymer with a larger number of QA groups. This phenomenon was also observed in literature, where a higher number of QA sites on phenylene rings in a poly(arylene ether sulfone) copolymer chain resulted in lower WA due to ionic clustering.⁸⁷

3.4. CO₂ sorption/desorption and kinetic modelling

MSS activity of polymers tested in an experimental setup (see **S.3**, Supporting Information for details on experimental setup) is shown in **Figure 4**. **Figure 4(a)** is a blank run showing the IRGA's reading of CO₂ levels in a closed system with varying environmental gas volume (e.g., humidity). A correction is applied on the experimental data (see **Equation S.1**, SI, for calculation) that accounts for the dilution of CO₂ caused by the introduction of water vapor. All polymers (**Figure 4(b-d)**) show distinct deviations from the blank run; specifically, an increase in the magnitude of the swing in CO₂ concentration occurs as the concentration of ammonium groups in the copolymer increases. The lower black curve shows the water concentration in parts per thousand, which is controlled using a dew point generator. The relative humidity is cycled between values of 8 ppt (~30% RH) and 25 ppt (~95% RH). As the water vapor concentration in the chamber increases the CO₂ concentration also rises, indicating the sample releases CO₂ under higher humidity conditions. Conversely, as the relative humidity in the chamber is decreased, the CO₂ concentration in the chamber also decreases, indicating CO₂ capture under dry conditions. Thus, the MSS

mechanism is satisfied. Also of note, desorption is performed spontaneously without extra heat supply as the system is maintained at room temperature.



^{*}Theoretical effective IEC is theoretical IEC/2 due to the nature of the MSS mechanism.

Figure 4 MSS mechanism (top left) and profiles for (a) Udel® 1700, (b) PAES-co-QAPAES[HCO $_3$](25), (c) PAES-co-QAPAES[HCO $_3$](50) and (d) PAES-co-QAPAES[HCO $_3$](75) ran with MSS of 8 – 25 ppt (30% RH to 95% RH at 22 °C) for 6 consecutive cycles of 2 h each (1 h sorption and 1 h desorption). The copolymer density, fractional free volume, water uptake, and ion exchange capacity are tabulated in the upper right.

Kinetic analysis is performed by fitting the data to pseudo-first-order (PFO) and pseudo-second-order (PSO) models in a 2.4 h CO₂ uptake test at 22 °C and 30% RH (**Figure 5**). We can draw some conclusions by looking at the trends in the data, discussed below. PAES-co-QAPAES[HCO₃-](25), PAES-co-QAPAES[HCO₃-](50) and PAES-co-QAPAES[HCO₃-](75) have theoretical effective IEC's of 0.45, 0.75, and 0.97 mmol/g, respectively (see **Equation S.2**, SI, for calculation). The CO₂ uptake values are

shown in **Figure 5**. Based on the PSO model, uptake values for PAES-co-QAPAES[HCO $_3$](25), PAES-co-QAPAES[HCO $_3$](50) and PAES-co-QAPAES[HCO $_3$](75) are 3.051 \pm 0.001, 29.793 \pm 0.022, and 31.579 \pm 0.009 µmol/g, respectively. Uptake values observed are significantly lower than uptakes reported for point source CO₂ sorption, which are 0.001 – 0.07 mol/g⁸⁸, but this is expected as the CO₂ partial pressure in air is much lower than point source CO₂ streams. Similarly, sorbents used for DAC via the MSS in the literature also exhibit uptake capacities in the range of 0.001 mol/g, but these comparisons are not entirely practical, as the experimental conditions such as temperature (influences on kinetics and isotherms), volume of closed systems (influences desorption CO₂ partial pressure) and extent of moisture swing (influences number of sites available) either vary or are not reported (see **Table S.9**, SI, for comparison of data reported in literature and this study). ^{13,89} The rate constants for PAES-co-QAPAES[HCO $_3$](25) and PAES-co-QAPAES[HCO $_3$](75) are similar, and about an order of magnitude faster than PAES-co-QAPAES[HCO $_3$](50).

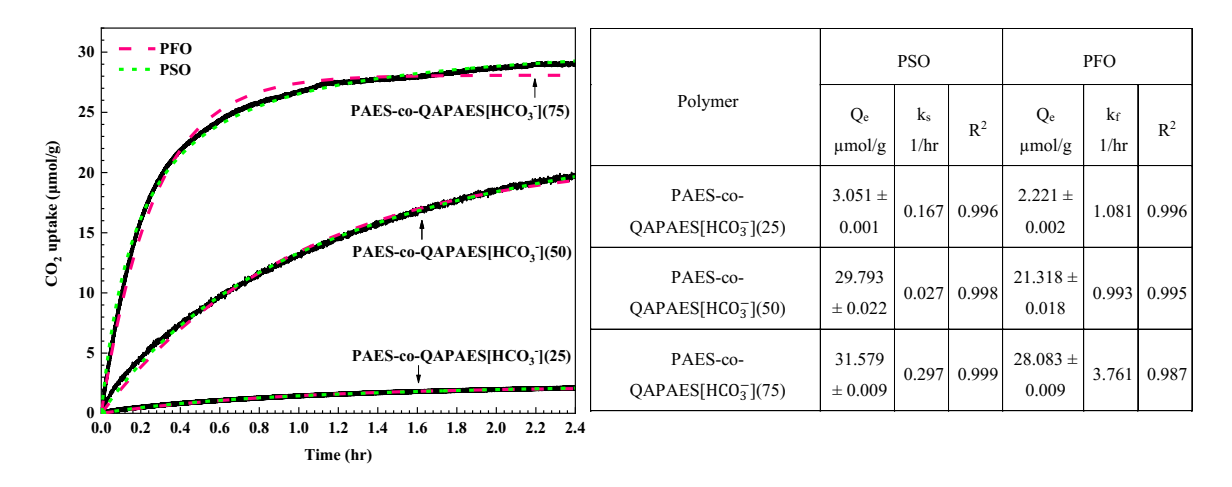


Figure 5 Experimental CO₂ uptake data and modeling of PFO and PSO at 22 °C and 30% RH. Better agreement is observed for PSO model for all samples, with increasing CO₂ sorption capacity with increasing IEC (QA functionalities).

The working capacity of the sorbents are much lower than their theoretical effective IEC, and the percent of site utilization changes with changes in the number of QA groups. We suspect the following arguments may be influencing lower working capacities and may be the foundation of future work. In general, water (humidity) can influence many aspects of the MSS process, in positive and negative ways. It may deactivate CO₂ capture sites through anion deprotonation, or the existence of a hydration layer

surrounding the hygroscopic QA groups, even when exposed to dry atmosphere, may interrupt the CO₂ capture process and cause diffusion constraints.^{21,90,91} Water present in the copolymers can promote ion transport and provide free protons for the reaction between CO₂ and sorbent. More investigations are required to elucidate the multiple roles of water on the MSS process and inform sorbent modifications to increase/decrease hydrophobicity. One way this is manifested in our work is the modest improvement in sorption capacity exhibited by PAES-co-QAPAES[HCO₃](75) relative to PAES-co-QAPAES[HCO₃](50). The former copolymer has a lower water uptake percentage but a larger fractional free volume, which highlights how the interplay of chemical reactions between the alkaline counterions with CO₂ and the polymer thermomechanical properties will dictate the material performance for DAC. Also, in the MSS process, two QA sites are simultaneously involved. In other words, to hold a divalent CO_3^{2-} ion, the distance between two QA ions should not be much larger than the size of one carbonate ion.²² Further evaluation is needed on the synthesized materials to explore these geometrical requirements and inform macromolecule structural features that locate ion exchange sites at appropriate distances. Finally, as shown herein, increasing the IEC does not necessarily optimize DAC performance. Block polymer structures might help retain mechanical properties while creating task-specific domains for the capture of CO₂. 92 These ideas are also employed to explain higher utilization of sites for 50% and 75% QA-functionalized (3.97% and 3.26%) site utilization (calculated as working capacity divided by IEC times 100)), respectively) versus 25% QAfunctionalized (0.68% site utilization), and, the discrepancy between utilization sites for 50% and 75% QAfunctionalized polymer.

4. CONCLUSIONS:

In this work, novel quaternary ammonium functionalized poly(arylene ether sulfones) are successfully synthesized through step growth reaction and subsequent post-polymerization modification reactions. Characterization of materials show the successful synthesis of high molecular weights polymers with amorphous morphology and randomly dispersed polymer segments. The degradation temperature of polymers is beyond operational temperatures (241 °C– 262 °C). The designed sorbents sorb CO₂ when dry

and desorb CO₂ when exposed to humidity without additional energy supply. Sorption/desorption cycles show the performance of materials is stable for six consecutive cycles. Nevertheless, the MSS process requires more in-depth analysis. The effect of purity of air and humidity, and weather conditions, seasonal temperature changes and wind speed on sorbent performance can be explored. Modification of material is expected to increase site utilization and CO₂ loading in MSS. Continuous DAC systems DAC may be developed after material optimization with dense free-standing membranes made from QA-functionalized poly(arylene ether sulfone). After material optimization, performance analysis may be performed to reach the DAC target of \$100/ ton CO₂ for large scale use.

5. Author Contributions:

Hoda Shokrollahzadeh Behbahani performed synthesis, SEC, ¹H NMR, TGA, DSC, MSS tests, data analysis and wrote the paper. Husain Mithaiwala contributed to polymer synthesis and cyclic contents analysis. Horacio Lopez Marques measured the WA of polymers with water vapor gravimetric sorption method. Winston Wang measured the density of polymers using a Helium pycnometer. Dr. Benny Freeman reviewed and edited the manuscript. Dr. Matthew D. Green was the Lead PI and supervisor on the project and reviewed and edited the manuscript.

6. Acknowledgements:

The authors gratefully acknowledge Prof. Klaus Lackner for his invaluable insights in the duration of this research. We also wish to acknowledge the support of the Center of Negative Carbon emissions (CNCE) at Arizona State University and Dr. Justin Flory, Dr. Jennifer Lynn Wade, Dr. Yuta Kaneko and Dr. Mani Modayil Korah for their valuable advice and interest in this work. We also wish to thank Allen Wright for his contribution to building the MSS testing setup.

The information, data, or work presented herein was funded in part by the Advanced Research Projects Agency-Energy (ARPA-E), U.S. Department of Energy, under Award Number DE-AR0001103. The views and opinions of authors expressed herein do not necessarily state or reflect those of the United

States Government or any agency thereof. Additional funding from NSF CBET 1836719 was used to support this work.

7. Supporting Information:

The Supporting Information is available online and contains descriptions of the experimental setup and calculations for MSS study, details of molecular weight analysis, details of true density measurements and molar volume, van der Waals volume and fractional free volume calculations.

8. Conflict of Interest Disclosure

None to disclose.

9. References:

- (1) Sanz-Pérez, E. S.; Murdock, C. R.; Didas, S. A.; Jones, C. W. Direct Capture of CO₂ from Ambient Air. *Chem. Rev.* **2016**, *116* (19), 11840–11876. https://doi.org/10.1021/acs.chemrev.6b00173.
- (2) Dvorak, M. T.; Armour, K. C.; Frierson, D. M. W.; Proistosescu, C.; Baker, M. B.; Smith, C. J. Estimating the Timing of Geophysical Commitment to 1.5 and 2.0 °C of Global Warming. *Nat. Clim. Chang.* **2022**, *12* (6), 547–552. https://doi.org/10.1038/s41558-022-01372-v.
- (3) Fawzy, S.; Osman, A. I.; Doran, J.; Rooney, D. W. Strategies for Mitigation of Climate Change: A Review. *Environ. Chem. Lett.* **2020**, *18* (6), 2069–2094. https://doi.org/10.1007/s10311-020-01059-w.
- (4) Navazi, F.; Sedaghat, A.; Tavakkoli-Moghaddam, R. A New Sustainable Location-Routing Problem with Simultaneous Pickup and Delivery by Two-Compartment Vehicles for a Perishable Product Considering Circular Economy. *IFAC-PapersOnLine* **2019**, *52* (13), 790–795. https://doi.org/10.1016/j.ifacol.2019.11.212.
- (5) Glier, J. C.; Rubin, E. S. Assessment of Solid Sorbents as a Competitive Post-Combustion CO₂ Capture Technology. *Energy Procedia* **2013**, *37*, 65–72. https://doi.org/10.1016/j.egypro.2013.05.086.
- (6) Cebrucean, D.; Cebrucean, V.; Ionel, I. CO₂ Capture and Storage from Fossil Fuel Power Plants. *Energy Procedia* **2014**, *63* (ii), 18–26. https://doi.org/10.1016/j.egypro.2014.11.003.
- (7) Rossing, T. D.; Chiaverina, C. J. *Sources of CO2*; Springer International Publishing: Cham, 2019. https://doi.org/10.1007/978-3-030-27103-9 8.
- (8) Ghahramani, A.; Pantelic, J.; Vannucci, M.; Pistore, L.; Liu, S.; Gilligan, B.; Alyasin, S.; Arens, E.; Kampshire, K.; Sternberg, E. Personal CO₂ Bubble: Context-Dependent Variations and Wearable Sensors Usability. *J. Build. Eng.* **2019**, *22* (September 2018), 295–304. https://doi.org/10.1016/j.jobe.2018.11.015.
- (9) The International Council on Clean Transportation (ICCT). Real Impact https://theicct.org/.
- (10) Carbon dioxide now more than 50% higher than pre-industrial levels https://www.noaa.gov/news-release/carbon-dioxide-now-more-than-50-higher-than-pre-industrial-levels.
- (11) Huang, L.; Krigsvoll, G.; Johansen, F.; Liu, Y.; Zhang, X. Carbon Emission of Global Construction Sector. *Renew. Sustain. Energy Rev.* **2018**, *81* (June), 1906–1916. https://doi.org/10.1016/j.rser.2017.06.001.
- (12) Lackner, K. S.; Grimes, P.; Ziock, H. Carbon Dioxide Extraction from Air: Is It an Option? In *24th Annual Technical Conference on Coal Utilization and Fuel Systems*; 1999.
- Wang, T.; Huang, J.; He, X.; Wu, J.; Fang, M.; Cheng, J. CO₂ Fertilization System Integrated with a Low-Cost Direct Air Capture Technology. *Energy Procedia* **2014**, *63*, 6842–6851. https://doi.org/10.1016/j.egypro.2014.11.718.
- (14) Kong, F.; Rim, G.; Song, M.; Rosu, C.; Priyadarshini, P.; Lively, R. P.; Realff, M. J.; Jones, C. W. Research Needs Targeting Direct Air Capture of Carbon Dioxide: Material; Process Performance Characteristics under Realistic Environmental Conditions. *Korean J. Chem. Eng.* **2022**, *39* (1), 1–19. https://doi.org/10.1007/s11814-021-0976-0.
- (15) Shi, X.; Xiao, H.; Azarabadi, H.; Song, J.; Wu, X.; Chen, X.; Lackner, K. S. Sorbents for the Direct Capture of CO₂ from Ambient Air. *Angew. Chemie Int. Ed.* **2020**, *59* (18), 6984–7006. https://doi.org/10.1002/anie.201906756.
- (16) Lackner, K. S.; Brennan, S. Envisioning Carbon Capture and Storage: Expanded Possibilities Due to Air Capture, Leakage Insurance, and C-14 Monitoring. *Clim. Change* **2009**, *96* (3), 357–378. https://doi.org/10.1007/s10584-009-9632-0.
- (17) Lackner, K.; Ziock, H.-J.; Grimes, P. Capturing Carbon Dioxide from Air. In *First International Sequestration Conference*; Alexandria, VA, 2001; pp 1–15.
- (18) Yang, H.; Singh, M.; Schaefer, J. Humidity-Swing Mechanism for CO₂ Capture from Ambient Air. *Chem. Commun.* **2018**, *54* (39), 4915–4918. https://doi.org/10.1039/C8CC02109K.
- (19) Shi, X.; Xiao, H.; Lackner, K. S.; Chen, X. Capture CO₂ from Ambient Air Using Nanoconfined

- Ion Hydration. *Angew. Chemie Int. Ed.* **2016**, *55* (12), 4026–4029. https://doi.org/10.1002/anie.201507846.
- (20) Shi, X.; Xiao, H.; Kanamori, K.; Yonezu, A.; Lackner, K. S.; Chen, X. Moisture-Driven CO₂ Sorbents. *Joule* **2020**, *4* (8), 1823–1837. https://doi.org/10.1016/j.joule.2020.07.005.
- Wang, T.; Lackner, K. S.; Wright, A. B. Moisture-Swing Sorption for Carbon Dioxide Capture from Ambient Air: A Thermodynamic Analysis. *Phys. Chem. Chem. Phys.* **2013**, *15* (2), 504–514. https://doi.org/10.1039/c2cp43124f.
- Wang, T.; Lackner, K. S.; Wright, A. Moisture Swing Sorbent for Carbon Dioxide Capture from Ambient Air. *Environ. Sci. Technol.* **2011**, *45* (15), 6670–6675. https://doi.org/10.1021/es201180v.
- (23) Kaneko, Y.; Lackner, K. S. Kinetic Model for Moisture-Controlled CO 2 Sorption. *Phys. Chem. Chem. Phys.* **2022**, *24* (35), 21061–21077. https://doi.org/10.1039/D2CP02440C.
- (24) He, H.; Li, W.; Zhong, M.; Konkolewicz, D.; Wu, D.; Yaccato, K.; Rappold, T.; Sugar, G.; David, N. E.; Matyjaszewski, K. Reversible CO₂ Capture with Porous Polymers Using the Humidity Swing. *Energy Environ. Sci.* **2013**, *6* (2), 488–493. https://doi.org/10.1039/C2EE24139K.
- (25) Wang, T.; Ge, K.; Chen, K.; Hou, C.; Fang, M. Theoretical Studies on CO2 Capture Behavior of Quaternary Ammonium-Based Polymeric Ionic Liquids. *Phys. Chem. Chem. Phys.* **2016**, *18* (18), 13084–13091. https://doi.org/10.1039/c5cp07229h.
- (26) Chintapalli, M.; Meckler, S.; Iftime, G.; Pandey, R.; Louie, M.; Shin Ming Beh, E. Tunable, Rapid Uptake, Aminopolymer Aerogel Sorbent for Direct Air Capture of CO₂. US20210370226A1, 2021.
- (27) Meckler, S. M.; Iftime, G.; Nallapaneni, A.; Van Overmeere, Q.; Keoshkerian, B.; Bulger, E.; Ho, A. S.; Zhu, C.; Rivest, J. B.; Chintapalli, M. Optically Transparent Polymer Aerogels Via Controlled Radical Polymerization. *ACS Appl. Polym. Mater.* **2022**, *4* (3), 1565–1569. https://doi.org/10.1021/acsapm.1c01854.
- (28) He, H.; Li, W.; Lamson, M.; Zhong, M.; Konkolewicz, D.; Hui, C. M.; Yaccato, K.; Rappold, T.; Sugar, G.; David, N. E.; Damodaran, K.; Natesakhawat, S.; Nulwala, H.; Matyjaszewski, K. Porous Polymers Prepared via High Internal Phase Emulsion Polymerization for Reversible CO₂ Capture. *Polymer (Guildf).* **2014**, *55* (1), 385–394. https://doi.org/10.1016/j.polymer.2013.08.002.
- (29) Wang, T.; Liu, J.; Fang, M.; Luo, Z. A Moisture Swing Sorbent for Direct Air Capture of Carbon Dioxide: Thermodynamic and Kinetic Analysis. *Energy Procedia* **2013**, *37*, 6096–6104. https://doi.org/10.1016/j.egypro.2013.06.538.
- (30) Wang, T.; Ge, K.; Chen, K.; Hou, C.; Fang, M. Theoretical Studies on CO₂ Capture Behavior of Quaternary Ammonium-Based Polymeric Ionic Liquids. *Phys. Chem. Chem. Phys.* **2016**, *18* (18), 13084–13091. https://doi.org/10.1039/C5CP07229H.
- (31) Hou, C.; Wu, Y.; Wang, T.; Wang, X.; Gao, X. Preparation of Quaternized Bamboo Cellulose and Its Implication in Direct Air Capture of CO₂. *Energy & Fuels* **2019**, *33* (3), 1745–1752. https://doi.org/10.1021/acs.energyfuels.8b02821.
- (32) Song, J.; Liu, J.; Zhao, W.; Chen, Y.; Xiao, H.; Shi, X.; Liu, Y.; Chen, X. Quaternized Chitosan/PVA Aerogels for Reversible CO₂ Capture from Ambient Air. *Ind. Eng. Chem. Res.* **2018**, *57* (14), 4941–4948. https://doi.org/10.1021/acs.iecr.8b00064.
- (33) Armstrong, M.; Shi, X.; Shan, B.; Lackner, K.; Mu, B. Rapid CO 2 Capture from Ambient Air by Sorbent-containing Porous Electrospun Fibers Made with the Solvothermal Polymer Additive Removal Technique. *AIChE J.* **2019**, *65* (1), 214–220. https://doi.org/10.1002/aic.16418.
- (34) Parzuchowski, P. G.; Świderska, A.; Roguszewska, M.; Rolińska, K.; Wołosz, D. Moisture- and Temperature-Responsive Polyglycerol-Based Carbon Dioxide Sorbents—The Insight into the Absorption Mechanism for the Hydrophilic Polymer. *Energy & Fuels* **2020**, *34* (10), 12822–12832. https://doi.org/10.1021/acs.energyfuels.0c02174.
- (35) He, H.; Zhong, M.; Konkolewicz, D.; Yacatto, K.; Rappold, T.; Sugar, G.; David, N. E.; Gelb, J.; Kotwal, N.; Merkle, A.; Matyjaszewski, K. Three-Dimensionally Ordered Macroporous Polymeric Materials by Colloidal Crystal Templating for Reversible CO₂ Capture. *Adv. Funct. Mater.* **2013**, 23 (37), 4720–4728. https://doi.org/10.1002/adfm.201300401.
- (36) Realff, M. J.; Min, Y. J.; Jones, C. W.; Lively, R. P. Perspective the Need and Prospects for

- Negative Emission Technologies Direct Air Capture through the Lens of Current Sorption Process Development. *Korean J. Chem. Eng.* **2021**, *38* (12), 2375–2380. https://doi.org/10.1007/s11814-021-0957-3.
- Wang, T.; Wang, X.; Hou, C.; Liu, J. Quaternary Functionalized Mesoporous Adsorbents for Ultra High Kinetics of Capture from Air. *Sci. Rep.* **2020**, No. 0123456789, 1–8. https://doi.org/10.1038/s41598-020-77477-1.
- (38) Muroyama, A. P.; Beard, A.; Pribyl-Kranewitter, B.; Gubler, L. Separation of CO₂ from Dilute Gas Streams Using a Membrane Electrochemical Cell . *ACS ES&T Eng.* **2021**, *1* (5), 905–916. https://doi.org/10.1021/acsestengg.1c00048.
- (39) Prajapati, A.; Sartape, R.; Rojas, T.; Dandu, N. K.; Dhakal, P.; Thorat, A. S.; Xie, J.; Bessa, I.; Galante, M. T.; Andrade, M. H. S.; Somich, R. T.; Rebouças, M. V.; Hutras, G. T.; Diniz, N.; Ngo, A. T.; Shah, J.; Singh, M. R. Migration-Assisted, Moisture Gradient Process for Ultrafast, Continuous CO₂ Capture from Dilute Sources at Ambient Conditions. *Energy Environ. Sci.* **2022**, 15 (2), 680–692. https://doi.org/10.1039/D1EE03018C.
- (40) Xu, M.; Xue, H.; Wang, Q.; Jia, L. Sulfonated Poly(Arylene Ether)s Based Proton Exchange Membranes for Fuel Cells. *Int. J. Hydrogen Energy* **2021**, *46* (62), 31727–31753. https://doi.org/10.1016/j.ijhydene.2021.07.038.
- Wang, J.; Wang, J.; Li, S.; Zhang, S. Poly(Arylene Ether Sulfone)s Ionomers with Pendant Quaternary Ammonium Groups for Alkaline Anion Exchange Membranes: Preparation and Stability Issues. *J. Memb. Sci.* **2011**, *368* (1–2), 246–253. https://doi.org/10.1016/j.memsci.2010.11.058.
- (42) Rambabu, K.; Bharath, G.; Arangadi, A. F.; Velu, S.; Banat, F.; Show, P. L. ZrO₂ Incorporated Polysulfone Anion Exchange Membranes for Fuel Cell Applications. *Int. J. Hydrogen Energy* **2020**, 45 (54), 29668–29680. https://doi.org/10.1016/j.ijhydene.2020.08.175.
- (43) Parodi, F. Polysulfones. In *Comprehensive Polymer Science and Supplements*; Elsevier, 1989; pp 561–591. https://doi.org/10.1016/B978-0-08-096701-1.00174-9.
- (44) Li, Y.; Cheng, J.; Zhang, J. A Newly Designed Dual-Functional Epoxy Monomer for Preparation of Fishbone-Shaped Heterochain Polymer with a High Damping Property at Low Temperature. *Macromol. Mater. Eng.* **2017**, *302* (5). https://doi.org/10.1002/mame.201600574.
- (45) Viswanathan, R.; Johnson, B. C.; McGrath, J. E. Synthesis, Kinetic Observations and Characteristics of Polyarylene Ether Sulphones Prepared via a Potassium Carbonate DMAC Process. *Polymer (Guildf)*. **1984**, *25* (12), 1827–1836. https://doi.org/10.1016/0032-3861(84)90258-1.
- (46) Hedrick, J. L.; Patsiga, R. A.; McGrath, J. E. Synthesis and Characterization of Sulfonated Poly(Arylene Ether Sulfones). *Am. Chem. Soc. Polym. Prepr. Div. Polym. Chem.* **1984**, *25* (2), 88–90.
- (47) Yang, Y.; Muhich, C. L.; Green, M. D. Kinetics and Mechanisms of Polycondensation Reactions between Aryl Halides and Bisphenol A. *Polym. Chem.* **2020**, *11* (31), 5078–5087. https://doi.org/10.1039/D0PY00740D.
- (48) Xu, J.; Boyer, C. Visible Light Photocatalytic Thiol-Ene Reaction: An Elegant Approach for Fast Polymer Postfunctionalization and Step-Growth Polymerization. *Macromolecules* **2015**, *48* (3), 520–529. https://doi.org/10.1021/ma502460t.
- (49) Christian, P. Polymer Chemistry. *Electrospinning Tissue Regen.* **2011**, 34–50. https://doi.org/10.1016/B978-1-84569-741-9.50002-1.
- (50) Wang, J.; Zhao, Z.; Gong, F.; Li, S.; Zhang, S. Synthesis of Soluble Poly (Arylene Ether Sulfone) Ionomers with Pendant Quaternary Ammonium Groups for Anion Exchange Membranes. **2009**, 8711–8717. https://doi.org/10.1021/ma901606z.
- (51) Burgess, S. K.; Mikkilineni, D. S.; Yu, D. B.; Kim, D. J.; Mubarak, C. R.; Kriegel, R. M.; Koros, W. J. Water Sorption in Poly(Ethylene Furanoate) Compared to Poly(Ethylene Terephthalate). Part 1: Equilibrium Sorption. *Polymer (Guildf)*. 2014, 55 (26), 6861–6869. https://doi.org/10.1016/j.polymer.2014.10.047.
- (52) Singh, A.; Freeman, B. D.; Pinnau, I. Pure and Mixed Gas Acetone/Nitrogen Permeation Properties

- of Polydimethylsiloxane [PDMS]. *J. Polym. Sci. Part B Polym. Phys.* **1998**, *36* (2), 289–301. https://doi.org/10.1002/(SICI)1099-0488(19980130)36:2<289::AID-POLB8>3.0.CO;2-M.
- (53) Dhoot, S. N.; Freeman, B. D. Kinetic Gravimetric Sorption of Low Volatility Gases and Vapors in Polymers. *Rev. Sci. Instrum.* **2003**, *74* (12), 5173–5178. https://doi.org/10.1063/1.1622978.
- (54) Moon, J. D.; Galizia, M.; Borjigin, H.; Liu, R.; Riffle, J. S.; Freeman, B. D.; Paul, D. R. Water Vapor Sorption, Diffusion, and Dilation in Polybenzimidazoles. *Macromolecules* **2018**, *51* (18), 7197–7208. https://doi.org/10.1021/acs.macromol.8b01659.
- (55) Yampolskii, Y.; Pinnau, I.; Freeman, B. D. *Materials Science of Membranes for Gas and Vapor Separation*; Yampolskii, Y., Pinnau, I., Freeman, B., Eds.; John Wiley & Sons, Ltd: Chichester, UK, 2006. https://doi.org/10.1002/047002903X.
- (56) Bondi, A. A. *Physical Properties of Molecular Crystals Liquids, and Glasses*; New York, Wiley, 1968.
- (57) Van Krevelen, D. W.; Te Nijenhuis, K. Volumetric Properties. In *Properties of Polymers*; Elsevier, 2009; pp 71–108.
- (58) Zur Theorie Der Sogenannten Adsorption Gelöster Stoffe. Zeitschrift für Chemie und Ind. der Kolloide 1907, 2 (1), 15–15. https://doi.org/10.1007/BF01501332.
- (59) Ho, Y. .; McKay, G. Pseudo-Second Order Model for Sorption Processes. *Process Biochem.* **1999**, 34 (5), 451–465. https://doi.org/10.1016/S0032-9592(98)00112-5.
- (60) Yang, Y.; Ramos, T. L.; Heo, J.; Green, M. D. Zwitterionic Poly(Arylene Ether Sulfone) Copolymer/Poly(Arylene Ether Sulfone) Blends for Fouling-Resistant Desalination Membranes. *J. Memb. Sci.* **2018**, *561*, 69–78. https://doi.org/10.1016/J.MEMSCI.2018.05.025.
- (61) Mielby, J.; Kegnæs, S. Epoxidation of Alkenes with Aqueous Hydrogen Peroxide and Quaternary Ammonium Bicarbonate Catalysts. *Catal. Letters* **2013**, *143* (11), 1162–1165. https://doi.org/10.1007/s10562-013-1088-1.
- (62) Kim, J. M.; Lin, Y.; Hunter, B.; Beckingham, B. S. Transport and Co-Transport of Carboxylate Ions and Ethanol in Anion Exchange Membranes. *Polymers (Basel)*. **2021**, *13* (17), 2885. https://doi.org/10.3390/polym13172885.
- (63) Dischinger, S. M.; Gupta, S.; Carter, B. M.; Miller, D. J. Transport of Neutral and Charged Solutes in Imidazolium-Functionalized Poly(Phenylene Oxide) Membranes for Artificial Photosynthesis. *Ind. Eng. Chem. Res.* **2020**, *59* (12), 5257–5266. https://doi.org/10.1021/acs.iecr.9b05628.
- (64) Rieman, W.; Walton, H. F. *Ion Exchange in Analytical Chemistry*; Elsevier, 1970. https://doi.org/10.1016/C2013-0-05561-2.
- (65) Hofmann, A. W. Von. XIV. Researches into the Molecular Constitution of the Organic Bases. *Philos. Trans. R. Soc. London* **1851**, *141*, 357–398. https://doi.org/10.1098/rstl.1851.0017.
- (66) Kricheldorf, H. R.; Böhme, S.; Schwarz, G.; Krüger, R.-P.; Schulz, G. Macrocycles. 18. The Role of Cyclization in Syntheses of Poly(Ether–sulfone)S. *Macromolecules* **2001**, *34* (26), 8886–8893. https://doi.org/10.1021/ma0102181.
- (67) Savariar, S.; Underwood, G. S.; Dickinson, E. M.; Schielke, P. J.; Hay, A. S. Polysulfone with Lower Levels of Cyclic Dimer: Use of MALDI-TOF in the Study of Cyclic Oligomers. *Desalination* **2002**, *144* (1–3), 15–20. https://doi.org/10.1016/S0011-9164(02)00282-5.
- (68) Carothers, W. H. Polymers and Polyfunctionality. *Trans. Faraday Soc.* **1936**, *32*, 39. https://doi.org/10.1039/tf9363200039.
- (69) Flory, P. J. Molecular Size Distribution in Linear Condensation Polymers 1. *J. Am. Chem. Soc.* **1936**, 58 (10), 1877–1885. https://doi.org/10.1021/ja01301a016.
- (70) Kricheldorf, H. *Polycondensation*; Springer Berlin Heidelberg: Berlin, Heidelberg, 2014; Vol. 9783642394. https://doi.org/10.1007/978-3-642-39429-4.
- (71) Wutz, C.; Kricheldorf, H. R. Molecular Weight Distribution of Linear Chains in Step-Growth Polymerization Under the Influence of Cyclization Reactions. *Macromol. Theory Simulations* **2012**, 21 (4), 266–271. https://doi.org/10.1002/mats.201100084.
- (72) Fawcett, A. H.; Mee, R. A. W.; McBride, F. V. A Monte-Carlo Study of Ring Formation and Molecular Configurations during Step Growth on a Lattice in Three Dimensions. *Macromolecules*

- 1995, 28 (5), 1481–1490. https://doi.org/10.1021/ma00109a020.
- (73) Kricheldorf, H. R.; Fritsch, D.; Vakhtangishvili, L.; Schwarz, G. Cyclic Ladder Polymers by Polycondensation of Silylated Tetrahydroxy-Tetramethylspirobisindane with 1,4-Dicyanotetrafluorobenzene. *Macromol. Chem. Phys.* **2005**, *206* (22), 2239–2247. https://doi.org/10.1002/macp.200500280.
- (74) Kricheldorf, H. R.; Schwarz, G. Cyclic Polymers by Kinetically Controlled Step-Growth Polymerization. *Macromol. Rapid Commun.* **2003**, 24 (56), 359–381. https://doi.org/10.1002/marc.200390063.
- (75) Kricheldorf, H. R.; Weidner, S. M. Copolyesters of Lactide, Isosorbide, and Terephthalic Acid-Biobased, Biodegradable, High- T g Engineering Plastics. *Macromol. Chem. Phys.* **2013**, *214* (6), 726–733. https://doi.org/10.1002/macp.201200612.
- (76) Kricheldorf, H. R.; Mix, R.; Weidner, S. M. Poly(Ester Urethane)s Derived from Lactide, Isosorbide, Terephthalic Acid, and Various Diisocyanates. *J. Polym. Sci. Part A Polym. Chem.* **2014**, 52 (6), 867–875. https://doi.org/10.1002/pola.27069.
- (77) Udel® Polysulfone Design Guide. *Solvay Specialty Polymers*; 2015; pp 1–84.
- (78) Zhang, Q.; Zhang, Q.; Wang, J.; Zhang, S.; Li, S. Synthesis and Alkaline Stability of Novel Cardo Poly(Aryl Ether Sulfone)s with Pendent Quaternary Ammonium Aliphatic Side Chains for Anion Exchange Membranes. *Polymer (Guildf)*. **2010**, *51* (23), 5407–5416. https://doi.org/10.1016/j.polymer.2010.09.049.
- (79) Ramgobin, A.; Fontaine, G.; Bourbigot, S. Thermal Degradation and Fire Behavior of High Performance Polymers. *Polym. Rev.* **2019**, *59* (1), 55–123. https://doi.org/10.1080/15583724.2018.1546736.
- (80) Choi, J.; Byun, Y. J.; Lee, S. Y.; Jang, J. H.; Henkensmeier, D.; Yoo, S. J.; Hong, S. A.; Kim, H. J.; Sung, Y. E.; Park, J. S. Poly(Arylene Ether Sulfone) with Tetra(Quaternary Ammonium) Moiety in the Polymer Repeating Unit for Application in Solid Alkaline Exchange Membrane Fuel Cells. *Int. J. Hydrogen Energy* **2014**, *39* (36), 21223–21230. https://doi.org/10.1016/j.ijhydene.2014.10.007.
- (81) Strasser, D. J.; Graziano, B. J.; Knauss, D. M. Base Stable Poly(Diallylpiperidinium Hydroxide) Multiblock Copolymers for Anion Exchange Membranes. *J. Mater. Chem. A* **2017**, *5* (20), 9627–9640. https://doi.org/10.1039/c7ta00905d.
- (82) El-Hibri, M. J. Sulfone Polymer Composition. EP1524297A1, 2005.
- (83) Polymer Processes Database. Bisphenol A Polysulfone https://polymerdatabase.com/polymers/bisphenolapolysulfone.html.
- (84) Pu, Z.; Xia, J.; Liu, X.; Wang, Q.; Liu, J.; He, X.; Zhong, J. Novel Polyethersulfone Dielectric Films with High Temperature Resistance, Intrinsic Low Dielectric Constant and Low Dielectric Loss. *J. Mater. Sci. Mater. Electron.* **2020**. https://doi.org/10.1007/s10854-020-04873-8.
- (85) Fox, T. G. Influence of Diluent and of Copolymer Composition on the Glass Temperature of a Polymer System. *Bull. Am. Phys. Soc.* **1956**, *1*, 123–132.
- (86) Dennis, J. M.; Fahs, G. B.; Moore, R. B.; Turner, S. R.; Long, T. E. Synthesis and Characterization of Polysulfone-Containing Poly(Butylene Terephthalate) Segmented Block Copolymers. *Macromolecules* **2014**, *47* (23), 8171–8177. https://doi.org/10.1021/ma501903h.
- (87) Weiber, E. A.; Jannasch, P. Ion Distribution in Quaternary-Ammonium-Functionalized Aromatic Polymers: Effects on the Ionic Clustering and Conductivity of Anion-Exchange Membranes. *ChemSusChem* **2014**, *7* (9), 2621–2630. https://doi.org/10.1002/cssc.201402223.
- (88) Osman, A. I.; Hefny, M.; Abdel Maksoud, M. I. A.; Elgarahy, A. M.; Rooney, D. W. Recent Advances in Carbon Capture Storage and Utilisation Technologies: A Review. *Environ. Chem. Lett.* **2021**, *19* (2), 797–849. https://doi.org/10.1007/s10311-020-01133-3.
- (89) Hou, C.; Wu, Y.; Jiao, Y.; Huang, J.; Wang, T.; Fang, M.; Zhou, H. Integrated Direct Air Capture and CO2 Utilization of Gas Fertilizer Based on Moisture Swing Adsorption. *J. Zhejiang Univ. A* **2017**, *18* (10), 819–830. https://doi.org/10.1631/jzus.A1700351.
- (90) Wang, T.; Liu, J.; Lackner, K. S.; Shi, X.; Fang, M.; Luo, Z. Characterization of Kinetic Limitations to Atmospheric CO₂ Capture by Solid Sorbent. *Greenh. Gases Sci. Technol.* **2016**, *6* (1), 138–149.

- https://doi.org/10.1002/ghg.1535.
- (91) Hsiao, E.; Barnette, A. L.; Bradley, L. C.; Kim, S. H. Hydrophobic but Hygroscopic Polymer Films-Identifying Interfacial Species and Understanding Water Ingress Behavior. *ACS Appl. Mater. Interfaces* **2011**, *3* (11), 4236–4241. https://doi.org/10.1021/am200894h.
- (92) Li, Y.; Liu, Y.; Savage, A. M.; Beyer, F. L.; Seifert, S.; Herring, A. M.; Knauss, D. M. Polyethylene-Based Block Copolymers for Anion Exchange Membranes. *Macromolecules* **2015**, *48* (18), 6523–6533. https://doi.org/10.1021/acs.macromol.5b01457.